



Development and characterization of antibody reagents for detecting nanoparticles

Journal:	<i>Nanoscale</i>
Manuscript ID	NR-ART-07-2015-004882.R1
Article Type:	Paper
Date Submitted by the Author:	19-Oct-2015
Complete List of Authors:	Ravichandran, Supriya; University of Rochester, Biomedical Engineering Sullivan, Mark; University of Rochester, Microbiology and Immunology Callahan, Linda; University of Rochester, Pathology and Laboratory Medicine Bentley, Karen; University of Rochester, Pathology and Laboratory Medicine DeLouise, Lisa; University of Rochester Medical Centre, Department of Dermatology

Development and characterization of antibody reagents for detecting nanoparticles

Authors: *Supriya Ravichandran*¹, *Mark A. Sullivan*², *Linda M. Callahan*³, *Karen L. Bentley*³,
Lisa A. DeLouise^{1,4*}

¹Department of Biomedical Engineering, University of Rochester, Rochester, New York 14642, USA. ²Department of Microbiology and Immunology, University of Rochester Medical Centre, Rochester, New York 14642, USA. ³ Department of Pathology and Laboratory Medicine, University of Rochester Medical Centre, 601 Elmwood Avenue, Box 626, Rochester, New York 14642, ⁴Department of Dermatology, University of Rochester Medical Centre, Rochester, New York 14642, USA.

*email: Lisa_DeLouise@urmc.rochester.edu

Keywords: nanoparticles, quantum dots, phage display, antibodies, scFv, skin

Abstract

The increasing use of nanoparticles (NPs) in technological applications and in commercial products has escalated environmental health and safety concerns. The detection of NPs in the environment and in biological systems is challenged by limitations associated with commonly used analytical techniques. In this paper we report on the development and characterization of NP binding antibodies, termed NProbes. Phage display methodology was used to discover antibodies that bind NPs dispersed in solution. We present a proof-of-concept for the generation of NProbes and their use for detecting quantum dots and titanium dioxide NPs *in vitro* and in an *ex vivo* human skin model. Continued development and refinement of NProbes to detect NPs that vary in composition, shape, size, and surface coating will comprise a powerful tool kit that

can be used to advance nanotechnology research particularly in the nanotoxicology and nanotherapeutics fields.

The global total market value for nanoparticles (NPs) in biotechnology is estimated to reach \$53.5B US dollars in 2017.¹ The increased formulation of NPs in therapeutics² and in consumer goods such as cosmetics,³ bicycle frames, tennis rackets, skis, and other sporting goods⁴ has raised human environmental health and safety (EH&S) concerns, especially for chronic low dose unintended occupational bodily exposures.⁵ NP safety concerns stem from their small size and high surface area to volume ratio, which imparts unique physiochemical properties and reactivity that are not present in the bulk form.⁶ When in contact with biological systems, these properties can alter tissue function⁷ and lead to potential toxicity.^{8,9} While metal oxide NPs such as TiO₂ and ZnO are formulated into ~70 % of all sunscreens¹⁰, the global market for QD NPs, which are commonly used in biomedical imaging,¹¹ biosensing¹² and photovoltaic¹³ applications, is expected to reach a value of \$1.1 billion in 2016.¹⁴

A key route for NPs to enter the body is through skin, which is the largest organ in the body. Existing results on NP skin penetration show varying trends that are largely dependent upon the NP size and surface chemistry,¹⁵⁻¹⁷ the skin model used,^{18, 19} the status of the skin barrier (intact or disrupted),^{19, 20} and the analytical techniques employed to detect the NPs.^{7, 16, 21, 22} While many studies report that for NPs to penetrate into the viable epidermis a defect is required in the stratum corneum barrier that maybe induced by tape stripping,¹⁹ dermabrasion,¹⁸ flexing^{18, 23} or UVR exposure,^{20, 24} however, contrasting literature reports exist^{25, 26}. It is important to note that the analytical techniques employed in these studies differed as would the NP detection limits which were typically not reported. For instance, it was observed based on TEM and tissue histology results that TiO₂ and ZnO NPs predominantly localize as aggregates in the stratum corneum (outer most layer of skin) but analysis using time-of-flight secondary ion mass spectrometry (TOF-SIMS) found high levels of both elemental Ti and Zn deep in the

epidermal layers,¹⁶ emphasizing the importance of considering the detection sensitivity of the analytical technique employed to detect NPs. Transmission electron microscopy (TEM) coupled with energy dispersive x-ray spectrometer (EDS) has superior nanoscale resolution and elemental detection capability that can provide a detailed analysis of NP localization in sub-cellular regions; however, a typical tissue slice used in TEM imaging is only 70-100 nm thick.²² Therefore, NPs present in tissue at very low levels may be missed due to sampling error. NPs may also be missed if elemental levels fall below the EDS instrument detection limit. To improve on the ability to detect NPs using TEM a colloidal silver enhancement strategy has been developed.²⁷ Here, colloidal silver selectively deposits onto metal/semiconducting NPs to produce larger particles that can be more easily identified and distinguished from spurious dark features. In previous work, we routinely observed higher QD presence in the viable epidermis using this procedure compared to histological analysis using fluorescence microscopy.^{20, 22} To achieve a more quantitative measure of NP presence, *in vivo* elemental organ analysis is typically performed on digested tissue samples using atomic absorption spectroscopy (AAS) or inductively coupled plasma mass spectrometry (ICP-MS). This approach provides a sensitive means to quantify the systemic transport of NPs. However, the tissue digestion process obfuscates the ability to distinguish transport of intact NP from soluble ion transport.²⁸ For some elements detection may be masked by interference from abundant trace metals or from endogenous elements such as carbon.¹⁶ The isotopic enrichment method outlined by Gulson et al.²⁹ can be used as a means to eliminate uncertainty pertaining to background levels of trace elements; however, this method is prohibitively expensive and impractical for routine NP studies. Confocal and fluorescence microscopy are also common techniques used to visualize the

presence of fluorescent NPs in tissues and while they allow for background noise reduction, the presence of NPs at low levels may still be obscured by tissue autofluorescence.²²

In order to unify published data on the topic of “Nanomaterials: environmental and health effects”, an action plan has been recommended in a recent review.³⁰ In this plan, one of the recommendations states that “an integral part of the harmonization of experimental methods is conclusive and feasible analytics; therefore, the development of appropriate and inexpensive analytical methods should be a part of funding programs”.³⁰ To this end and with a goal to better understand NP skin penetration, we have undertaken an effort to develop a simple technique that can provide information on both the NP presence and form³¹ in the environment and in a biological milieu, which can be used in conjunction with existing quantitative techniques. Here we present our initial efforts to develop antibody reagents that bind NPs (NProbes) using phage display technology. Phage display is a common method used to discover protein or peptide binders to a wide variety of targets. Typically, the nucleotide sequence encoding a peptide is fused to the phage coat protein gene allowing the peptide to be displayed on the phage exterior.³² A library of phage displaying unique peptides is created and an affinity based selection technique (bio-panning) is used to discover binders. Phage display technology has been successfully used to isolate peptides recognizing inorganic metals³³⁻³⁶, metal oxides³⁷⁻³⁹ and semiconductors.⁴⁰ In this work we use an antibody phage library which offers more diversity in terms of binding surface to discover more selective and high affinity reagents based on shape as well as composition. While very little is currently known about the ability of the immune system to recognize NPs^{41,42}, NP immunogenicity is not a requirement for enrichment of antibody binders using *in vitro* display technology as we are working with a preexisting library of human antibodies and do not rely on an *in vivo* B cell immune response to occur.

In this work NProbes were selected from a phage library consisting of $\sim 2 \times 10^9$ unique single chain variable fragment (scFv) antibodies each displayed monovalently on the minor pIII coat protein of M13 filamentous phage. This library has been used by us previously to generate scFvs against proteins⁴³ and cell surface antigens.⁴⁴ A key difference from our prior work is that here we have developed protocols to conduct bio-panning on NPs dispersed in solution rather than the standard method of immobilizing the target onto a substrate.⁴⁵ In this work the scFv antibodies were engineered with a peptide FLAG tag (DYKDDDDKL) to enable secondary detection/amplification of NP presence in tissue sections using standard immunohistochemistry (IHC) staining with an enzymatic reporter. Herein, we demonstrate a proof-of-concept for NProbe generation and their use for detecting QDs and TiO₂ NPs using *in vitro* assays and *ex vivo* human skin models.

Results and Discussion

Selection of binders to QDs and TiO₂ using phage display

For NProbe discovery we used glutathione-coated (GSH) QDs (CdSe/ZnS core/shell) and TiO₂ NPs (Evonik/Degussa, 80% anatase and 20% rutile crystal, ~ 21 nm primary particle size). We selected the GSH-QDs for their superior stability to resist agglomeration in water and buffer systems compared to other commonly used water soluble coatings such as dihydrolipoic acid (DHLA) (**Supplementary Figure S1**).⁴⁶ The hydrodynamic diameter and polydispersity of the GSH-QDs measured in water using dynamic light scattering (DLS) were 14.1 ± 2.5 nm and 0.33 ± 0.06 , respectively and they were negatively charged (-22.82 mV) as determined from zeta potential measurements (pH= 5.3-5.6). The Evonik TiO₂ was selected because of its wide use in commercial skin care products.⁴⁷ TiO₂ NPs dispersed in water form aggregates that range from ~ 100 nm to ~ 1.5 μ m when visualized under TEM (**Supplementary Figure S1**). NProbes to

GSH-QDs and TiO₂ NPs were isolated using affinity-based bio-panning which involves mixing the target NPs with the phage library. The GSH-QDs (400 μl, 100 nM) and the TiO₂ NPs (400 μl, 0.5 mg/ml) were diluted in tris-buffered saline (TBS) and mixed with the phage library (100 μl, ~10¹² phage/mL in TBS plus 0.5% casein) with gentle agitation. In the TBS buffer system the GSH-QDs exhibit a much lower tendency to agglomerate than the TiO₂ as seen in TEM images (**Supplementary Figure S1**). The hydrodynamic diameter and polydispersity of the GSH-QDs in TBS was found to be 25.2 ± 1.54 nm and 0.40 ± 0.03, respectively and they were negatively charged similar to the GSH-QDs in water. For GSH-QD panning the phage input library was pre-centrifuged (Optima TLX ultracentrifuge, Beckman Coulter) at 116,000 g (65,000 rpm) to pellet phage agglomerates. After incubation for 2 h at room temperature, the NP/phage mixtures were centrifuged to pellet the NPs with bound phage. The GSH-QD/phage mixture was centrifuged at 83,000 g (55,000 rpm) for 10 min and the TiO₂/phage mixture was centrifuged at 1300 g (4000 rpm) for 5 min. After removing unbound phage in the supernatant, the pellets were resuspended in TBS containing 0.05% Tween-20 (TBST). Wash cycles of centrifugation and re-suspension in TBST were repeated 5 times, following which the pellet was washed once in deionized water. After washing, the bound phages were eluted from the NPs using 0.1 M glycine (pH 2.2) and neutralized using 2 M Tris base. The titer of the eluted phage was quantified by transduction of ampicillin-resistant TG1 *Escherichia coli* host cells and the resulting colonies were counted. A phage pool for the next round of enrichment was generated by transduction of 20-100% of the previous round eluate. After overnight incubation, the pooled transductants were grown at 37 °C, infected with VCS M13 helper phage, and grown overnight at 30 °C. Phage stocks were prepared for the next round of panning by polyethylene glycol (PEG) precipitation. Typically, 4 rounds of panning were necessary to enrich for specific binders to NPs, after which a BstNI fingerprinting

analysis was performed. The presence of identical restriction enzyme patterns among the tested clones was taken as evidence of specific enrichment as we have previously shown.⁴⁴ The BstNI digests of 12 randomly selected clones following four rounds of NP panning typically found pattern repeats indicating 17-25% clonal abundance (**Supplementary Figure S2**). This was increased to >50% after five rounds of panning. Phage clones from the enriched populations, termed GSH43 ϕ and Ti49 ϕ , were selected for testing. It is important to note however, that the most abundant phage clones may not be strongest binders or exhibit the highest selectivity. Ongoing studies seek to characterize the binding affinity and selectivity of additional clones identified. The amino acid sequences of the scFvs for the two phage clones are given in **Supplementary Table 1**. It is interesting to point out that the CDR regions for both the GSH43 and the Ti49 scFvs are comprised of a high percentage of polar uncharged amino acids (serine and asparagine); 30% and 32%, respectively. Surprisingly, the CDR regions lack a preponderance of cysteines (<3%) and histidines (<1%) which typically are enriched in metal ion binding peptides.⁴⁸ This suggests an alternative mechanism is important for scFv antibodies binding to NPs. The GSH43 ϕ and Ti49 ϕ phage clones and their respective purified scFv antibodies were freshly prepared and used for *in vitro* verification of target binding and cross reactivity testing to similar and dissimilar materials which we discuss next.

Verification of NP binding *in vitro* using phage clones

In vitro assays were conducted to quantify the binding of the GSH43 ϕ and Ti49 ϕ clones to their respective NP targets and to test their cross reactivity binding to other NPs and to negative control phage clones including interleukin-12 (IL-12 ϕ), lactoferrin (LF ϕ), human GRP78 (BiP ϕ) and a 15 amino acid (PVSP(ps)SQKLKRKAEEDPE) peptide (Npep ϕ). First, we used a phage centrifugation titer assay to assess binding. Here, the NPs were mixed with the GSH43 ϕ , Ti49 ϕ

or IL-12 ϕ clones for 2 h at room temperature. After removal of unbound phage by centrifugation, the pellet was washed 5 times with TBST buffer, after which the phages were eluted and the titers quantified as discussed above. Results for the GSH43 ϕ and Ti49 ϕ clones consistently showed a 10-fold and 100-fold increase in binding to their target NP, respectively relative to the IL-12 ϕ negative control (**Supplementary Figure S3**). The lower enrichment value observed for the GSH43 ϕ likely results from the precipitation of unbound phage during the ultracentrifugation step causing higher background counts in the colony assay despite our efforts to pre-centrifuge the phage to clear aggregates. These values are nonetheless in accordance with an 8-fold enrichment that was reported for isolating peptides against solid ZnO substrates using phage display.³⁸ To show that the phage clones exhibit sequence specific binding we exchanged the light chain of GSH43 ϕ clone with the light chain of IL-12 ϕ and the hybrid phage was tested for binding to the GSH-QDs. This manipulation reduced the hybrid phage binding to the GSH-QDs by a factor of 4. To further verify phage binding we conducted TEM analysis. The GSH-QDs were mixed separately with the GSH43 ϕ clone and the IL-12 ϕ negative clone. Similarly, the TiO₂ NPs were mixed separately with the Ti49 ϕ clone and the IL-12 ϕ negative clone. After a 2 h incubation at room temperature the four samples were washed to remove unbound phages using the centrifugation procedure described above. The pellets were re-suspended in TBS buffer and prepared for TEM analysis. Results (**Figure 1 and Supplementary Figure S4**) show evidence for Ti49 ϕ bound to TiO₂ NPs (black arrows, **Figure 1a**), whereas the IL-12 ϕ negative clone did not (**Figure 1b**). TEM results also show the GSH43 ϕ bound to the GSH-QDs causing phage clustering (**Figure 1c**), whereas the IL-12 ϕ negative phage did not (**Figure 1d**). The apparent association of the GSH-QD with the major coat protein (PVIII) is a likely artifact of the harsh ultracentrifugation process which may cause QDs to dislodge and become trapped in the

phage pellet that is resuspended on the TEM grid. This does not happen in the control phage due to lack of GSH-QD binding in the solution phase.

To test for potential cross-reactivity binding to similar and dissimilar NPs that vary in core composition and surface coating we conducted phage titer assays using the centrifugation method and a custom plate titer assay. Results from the centrifugation titer assay (**Figure 2a and Supplementary Figure S5**) indicate that the Ti49 ϕ clone binds to the TiO₂ (Evonik P25) and to TiO₂ NPs from a secondary vendor (Sigma Aldrich Inc., #677469) whereas negligible binding to Au-powder (<10 μ m particle size Sigma Aldrich Inc., #326585), citrate coated 20 nm Au NPs (Sigma Aldrich Inc., #753610) and carboxylated multi-walled carbon nanotubes (CNT-MWSusp-100, NanoLab, Inc.) is seen. Additionally, the Ti49 ϕ bound other TiO₂ NPs including TiO₂-anatase crystalline form (TiO₂-A, 32 nm size, Alfa Aesar) and TiO₂-rutile crystalline form (TiO₂-R, ~200 nm size, DuPont) demonstrating universal recognition of all forms of TiO₂ NPs (**Figure 2b**). Highest binding was observed to TiO₂-R potentially attributing to its larger particle sizes compared to the other forms (**Supplementary Figure S6**). The centrifugation titer assay was also used to test the cross reactivity binding of the GSH43 ϕ clone to the carboxylated CNTs and the citrated 20 nm Au NPs which showed negligible binding similar to IL-12 ϕ negative control (**Figure 2c and Supplementary Figure S5**).

To evaluate the cross reactivity binding of the GSH43 ϕ clone to QDs with similar core composition (ZnS/CdSe core/shell) but different coating chemistries we developed a plate titer assay to minimize background signal that results from inadvertent precipitation of unbound phage using ultracentrifugation separation. Following a literature protocol,⁴⁹ high binding 96 well plates were treated with 2% BSA prior to depositing the QDs. The QDs (50 μ l of a 50 nM

solution in sodium bicarbonate buffer) were added to the wells and allowed to incubated overnight at 4 °C with gentle agitation. The deposition and adherence of QDs before and after the multiple washing steps (7 TBST washes, 1 water wash) was confirmed using a handheld UVR light source (**Supplementary Figure S7**). Prior to conducting cross reactivity studies we first validated the binding of the GSH43 ϕ to immobilized GSH-QDs relative to empty vector phage containing the his6 and flag tags. No binding was observed for the empty vector phage, whereas GSH43 ϕ displayed a 200-fold more binding to GSH-QDs over phage control (**Supplementary Figure S8**). Moreover, the GSH43 ϕ bound the immobilized GSH-QDs in a dose dependent manor (**Supplementary Figure S8**). These results provided confidence that the plate titer assay could be used to examine NP cross reactivity binding. Results from the plate titer assay (**Figure 2c**) show that GSH43 ϕ (upon elution with glycine pH 2.2) binds to GSH-QD (25.2 nm and negatively charged), Invitrogen QDs (Inv-QD, Invitrogen ITK™ 565-QDs, 10 nm and negatively charged), and PEI-QD (23 nm and positively charged)⁴⁶ but minimal binding to the DHLA-QD (14 nm and negatively charged) is observed. These data suggest that QD binding in the phage format is not specific to the GSH coating or to surface charge. Moreover, using the plate titer assay (**Figure 2a and Supplementary Figure S9**) we found that Ti49 ϕ did not bind GSH-QDs confirming the absence of cross-reactivity of the Ti49 ϕ clone to GSH-QDs. To confirm these results we next examined the scFv binding to similar and dissimilar materials which is the intended NProbe format.

Verification of NP binding *in vitro* using scFvs

To examine the scFv binding characteristics we generated soluble His-tagged scFv protein that was affinity purified and characterized by SDS-PAGE gels to verify the purity was >95% (**Supplementary Figure S10**). To examine scFv binding to similar and dissimilar materials we first conducted dot blot assays to test the binding of the GSH43-scFv, the Ti49-scFv and the BiP-scFv (negative control) to GSH-QDs, Au NPs and CNTs that were spotted on a nitrocellulose membrane (**Figure 3a(i)-3a(iii), left column**). Similar to the phage binding studies (**Figure 2c**), the GSH43-scFvs showed high specific binding to the GSH-QDs indicated by the dark chemiluminescent spot formed (**Figure 3a(i), right column**). GSH43-scFv did not bind Au NPs (pink spot, center) or CNTs (black spot, right). The negative control BiP-scFv (**Figure 3a(ii)**) and the Ti49-scFv (**Figure 3a(iii)**) did not bind the GSH-QDs, the Au NPs or the CNTs. To test the GSH43-scFv binding to similar core materials but with different coating ligands we spotted GSH-QDs, Inv-QDs, DHLA-QDs and PEI-QDs on a nitrocellulose membrane (**Figure 3a(iv), left column**). Chemiluminescence detection of scFv binding using HRP (**Figure 3a(iv), right column**), shows that GSH43-scFvs bind GSH-QDs and DHLA-QDs, but not Inv-QDs and PEI-QDs. The negative control NT3-scFvs (**Figure 3a(v)**) showed only a faint background staining to all these QDs. The lack of GSH43-scFv binding to the PEI-QDs is in contrast to the strong binding observed in the phage format (**Figure 2c**). We attribute this to nonspecific binding of the positive PEI-QDs to the M13 phages which carry a high negative surface charge.⁵⁰ The lack of GSH43-scFv binding to the negative charged Inv-QD is also in contrast to the phage format results (**Figure 2c**). We attribute this to differences in binding affinity, as from dot blot concentration studies we did observe strong binding of the GSH-scFv to the Inv-QD with increasing GSH-scFv concentration (5-20 $\mu\text{g/mL}$) with a continued absence of binding to PEI-QDs (**Supplementary Figure S11**). The binding of GSH43-scFv to DLHA-QDs appears much

stronger than in the plate titer assay (**Figure 2c**) which may suggest the QD coating affects adherence to BSA coated plate. Over all, these results suggest that the GSH-scFv recognizes QDs with a similar core/shell composition but with different binding affinity which is also likely modulated the composition and liability of the surface ligand coating. Binding of GSH43-scFv to GSH-QDs was further confirmed using dynamic light scattering (DLS) with the BiP-scFv as the negative control. Here, the GSH-QDs were mixed with the scFvs at room temp for 2 h and ultra-centrifuged washed as discussed above. GSH-QDs in TBS buffer alone were also taken through the ultra-centrifugation wash and re-suspension steps for comparison. The hydrodynamic diameter of the GSH-QDs with bound GSH43-scFvs (~651 nm) was ~1.5-fold larger than that of BiP-associated GSH-QDs and ~2.5-fold GSH-QDs in TBS with statistical significance (**Supplementary Figure S12**). This data suggests that GSH-QDs bind to the GSH43-scFv despite their tendency to agglomerate in TBST. As further proof we conducted Image Stream flow cytometry measurement using anti-FLAG coated agarose beads. Beads coated with GSH43-scFv show intense QD fluorescence signal relative to beads exposed to GSH-QDs only, which showed no fluorescence signal. Only weak background fluorescence was detected following exposure of GSH-QDs to beads coated with negative control BiP-scFv (**Supplementary Figure S13**). We did not test the binding of the Ti49-scFv to TiO₂ NPs by dot-blot analysis as the presence of the NPs on the nitrocellulose membrane could not be verified by color. Hence, to confirm Ti49-scFv binding we dried the TiO₂ NPs onto a glass slide and used confocal microscopy to quantify the presence of fluorescein isothiocyanate (FITC)-conjugated anti-FLAG reporter. Images (**Figure 3b(i)**) were captured under bright-field and fluorescence. A control slide without TiO₂ NPs showed no background staining (**Supplementary Figure S14**). ImageJ (NIH) was used for analysis of line profiles of three regions of interest (ROIs) and the

results averaged. Although a slight background signal was detected for Npep-scFv on TiO₂ the quantification clearly shows a significant difference in the level of Ti49-scFv binding to TiO₂ NPs compared to negative control ($p < 0.05$, student's unpaired t-test, **Figure 3b(ii)**).

Validation of scFvs to detect NPs in a biological milieu

The main motivation for developing NProbe reagents is to facilitate the detection of NPs in biological systems in their particulate form. Existing studies of NP skin penetration have highlighted the need to consider the detection limits of the analytical techniques used as well as the assay protocol in drawing definitive conclusions about the NP skin penetration.^{16, 22} Having developed and characterized NProbe binding reagents to TiO₂ and QD NPs using *in vitro* assays, we next sought to test their ability to detect NPs in a biological milieu. First, we immobilized GSH-QDs on a glass slide coated with collagen, which is a key component of skin, and tested binding to GSH43-scFvs relative to a negative control (Npep-scFv) using confocal microscopy. We observed strong specific GSH43-scFvs binding to the GSH-QDs as indicated by the Pearson's co-localization coefficient of 0.65 (**Supplementary Figure S15**). GSH43-scFvs did not bind collagen films without containing QDs (data not shown). Next, we tested the ability of the scFv to detect NPs in fresh *ex vivo* human skin. NPs were topically applied to fresh *ex vivo* human using established protocols.¹⁹ Following NP skin exposure the tissue was cryo-sectioned for immuno-histochemical (IHC) analysis using NProbes and a secondary anti-FLAG reporter conjugated to an alkaline phosphatase (AP). Skin slices were pre-treated with levamisole (5 μ M) to eliminate endogenous phosphatase activity. **Figure 4** shows bright-field and fluorescent images of a skin section following a 24 h application GSH-QDs to the stratum corneum and a

control sample (no QD exposure). The control sample shows negligible AP staining (**Figure 4a**) indicating the absence of non-specific GSH43-scFv binding to the skin sections. In contrast, the skin sample exposed to GSH-QDs shows numerous punctate areas of strong AP staining in bright-field (**Figure 4b**). Observation of this skin section under fluorescence imaging shows a dense cluster of QDs (**Figure 4c**) that co-localizes with AP staining (blue arrows, **Figure 4b inset**). However, based on fluorescence imaging (**Figure 4c**) the detection of GSH-QD presence in skin is suggested to be far less than that suggested by AP staining. Using ImageJ software the fluorescence image can be threshold enhanced (**Figure 4d**) which reveals many more potential instances of QDs in the skin tissue; but as previously noted²² it is difficult to unambiguously distinguish the QDs from tissue autofluorescence artifacts. Results from AP staining (**Figure 4b**) however, clearly demonstrate the utility of NProbes to overcome this challenge. The AP staining identifies many areas that co-localize with high fluorescence (black arrows, **Figures 4b and 4d**). Additionally, we observed regions with strong AP staining with corresponding regions that do not show presence of QD fluorescence (red arrows, **Figures 4b and 4d**). This suggests that NProbes can identify QDs whose fluorescence cannot be detected over background. To validate that the areas of strong AP staining do indeed contain QDs we used laser capture microdissection (LCM) microscopy to isolate portions of the tissue sample by catapulting them into AdhesiveCap™ microfuge tubes, which were then assayed for elemental cadmium (Cd) using atomic absorption spectroscopy (AAS). Initial studies were conducted on a skin sample with a high QD presence introduced by dermal injection to ensure Cd levels exceeded the AAS detection limit of detection (LOD) equal to 7 pg/ml. The control skin sample (no QDs) again showed no discernable AP staining and no visible fluorescence QD signal (exposure time: 800 ms) (**Supplementary Figure S16**). In contrast, strong AP staining is seen under bright-field in

the dermis where GSH-QDs were injected as shown in **Figure 5a** with the corresponding QD fluorescence before dissection shown in **Figure 5b**. The portion of the skin marked for dissection is enclosed in the blue dotted area (**Figure 5c**). The portion remaining after catapult is shown in **Figure 5d**. AAS analysis of the tissue areas where strong QD fluorescence was co-localized with AP staining was performed to confirm the presence of Cd. Results indicated detection of 214 ng/mL of Cd.

Having demonstrated the ability of the LCM/AAS techniques to detect QD presence in the positive control sample, we proceeded to use this methodology to confirm the presence QDs in epidermal regions that exhibit strong AP staining following topical QD application on tape stripped skin (**Supplementary Figure S17**). Initial measurements of individual ROIs in tissue sections showed levels of Cd <LOD using AAS. However by combining six ROIs with strong AP staining we measured 108 pg/mL Cd, which is ~100 times above the LOD indicating the presence of QDs in these regions. The Cd level measured from six random ROI collected and combined from the control sample (no QD) was 8.5 pg/mL, which is near the instrument LOD (7 pg/ml) and may indicate the presence of endogenous Cd derived dietary sources which is more readily detected in the liver.^{15, 24} In addition, we collected and combined six ROIs with strong AP staining that lacked discernible QD signal under fluorescence imaging. AAS analysis measured 18 pg/mL Cd, which is above the instrument LOD and ~10 times higher than the endogenous Cd measured in the skin of the control (no QDs). These results demonstrate a proof-of-principle that NProbes can enable the detection of QDs (strong AP staining in bright field) present at low levels using simple IHC techniques.

We further sought to demonstrate the utility of NProbes by examining the penetration of nonfluorescent TiO₂ NPs through the human skin barrier using the Ti49-scFvs. The TiO₂ NPs (Evonik) were applied to intact skin in water and we also examined a TiO₂ containing commercial sunscreen (Eucerin SPF15). Results for both consistently show strong AP staining confined mainly to the upper layers of the stratum corneum (**Figure 6a**) relative to the control (no TiO₂ NPs) which did not show AP staining (**Figure 6b**). In some samples, we occasionally observed areas with mild punctate staining beneath the stratum corneum (**Figure 6a**, blue arrows) suggesting that TiO₂ NPs may have penetrated the stratum corneum barrier. Attempts to confirm the presence of TiO₂ NPs in tissue using AAS proved however, unsuccessful due to difficulties in dissolving TiO₂ for elemental analysis and a poor AAS detection sensitivity for Ti ions. Therefore, we attempted to examine the epidermal regions exhibiting light blue staining for the presence of TiO₂ particles using SEM. First, regions of dark staining in a control sample (TiO₂ applied directly to dermis for 24 h) were analyzed to visualize the morphology of TiO₂ NPs in the tissue milieu (**Supplementary Figure S18**). In this control tissue sample individual TiO₂ NPs could be readily discerned as part of larger aggregates. However, SEM analysis of several experimental skin samples exhibiting light blue staining in the epidermis and dermis were less conclusive as individual particles in the TiO₂ aggregates were harder to discern (**Supplementary Figure S19**). We were also unable to detect Ti ions in these regions using SEM/EDX. This is not unexpected however; as we estimate our TiO₂ EDX detection limit to be 0.5-5 $\mu\text{g}/\text{cm}^2$ which likely far exceeds the TiO₂ NP presence in these skin samples. Nevertheless, we are able to conclude that our results are consistent with the preponderance of recent literature investigating of TiO₂ NP skin penetration using different animal models,^{17, 20, 51,}

⁵² that significant penetration of beyond the stratum corneum is likely hindered by the high tendency of TiO₂ NPs to agglomerate.

Conclusions

In summary, using phage display technology we have discovered and characterized for the first time scFv antibody reagents that bind GSH-QDs and TiO₂ NPs and we have further demonstrated a proof-of-principle that these NProbe reagents can be used to simply detect NPs in skin using the standard immuno-histochemical technique. This work is unique in our approach to bio-pan on NPs dispersed in solution. Typically phage display requires the target to be immobilized onto a solid support by chemical coupling ⁵³ or non-covalent adsorption to a hydrophobic surface.⁵⁴ A previous study ⁴⁹ reported isolation of peptides using phage display that bind QDs immobilized on protein (gelatin)-coated polystyrene plates. However, when we immobilized QDs on gelatin and performed enrichments, only clones that bound gelatin were found. This phenomenon has been previously reported, where often off-target unrelated clones are enriched that bind to other components in the screening system rather than the target itself.⁵⁵ In fact, phage binding to components other than the target such as the solid phase (plastic, plates), substances used for blocking (BSA, milk) and capturing agents may predominate during rounds of bio-panning.⁵⁵ We also observed this in our efforts to pan on QDs immobilized to BSA coated plate which only generated binders to BSA. Hence, our solution phase panning approach helps to minimize occurrences of false positives and favors identification of clones recognizing the NPs dispersed in solution. It is clear however, from the data presented that the phage are panned against NP aggregates and that shape must be a key recognition element as the expected

metal binding amino acids are not predominant in the antibody CDR regions. Moreover, the enrichments values (10 to 100 fold) are less than expected for typical phage panning on proteins bound to a plate (>1000 fold). A plausible explanation is that the scFv “recognition epitope” varies dynamically in the panning process due to agglomeration. Future studies are planned to investigate this.

In this proof-of-concept study we demonstrated the utility of scFv antibodies to detect GSH-QDs and TiO₂ NPs in both *in vitro* and in the *ex vivo* human skin model. The scFvs isolated did not bind dissimilar materials tested, namely Au NPs, Au powder or CNTs. Several controls were included to validate binding including the use of random scFvs selected from the library and ‘no-NP’ controls in all experiments. The data presented herein for non-fluorescent TiO₂ detection validates the preponderance of current literature, which reports TiO₂ NPs agglomerates predominantly localize in the upper layers of the stratum corneum. However, we do observed instances of mild AP staining below the stratum corneum both for skin application of TiO₂ NPs from water and from a TiO₂ containing commercial sunscreen (Eucerin SPF 15). In these regions SEM studies confirmed the presence of structures that morphologically resemble TiO₂ aggregates suggesting possible presence in viable skin layers. However, efforts to detect the elemental Ti (EDX) proved inconclusive. In the QD studies we were able to confirm that instances of AP staining in the epidermis with and without a co-localized fluorescent signal did contain elemental Cd. Hence, it is likely that the instances of mild AP staining in the epidermis on TiO₂ treated skin (albeit less frequent than in QD treated skin) do indeed contain NPs. It is not unexpected that some TiO₂ NPs could penetrate through defects in the stratum corneum barrier.

In summary, we have discovered scFv antibodies that can bind to NPs and we show the advantage of using enzymatic reporting to amplify the detection NPs in skin. Our methodology

can be further exploited to develop NProbes for binding other NP types thereby providing an expansive tool kit that can complement other techniques to further our understanding of NP interactions in biological systems from a toxicology and therapeutic perspective. NProbes antibodies will be particularly advantageous for detecting non-fluorescent NPs using cost-effective and common imaging techniques. Therefore, we expect that NProbes can be advanced and used in conjunction with conventional techniques to overall improve NP detection abilities in tissues and other biological systems. In future studies we will seek to discover the mechanisms of NP scFv binding and how binding affinity and selectivity relate to NP agglomeration. In addition we will construct scFv-Fc fusion proteins which will provide more stable reagents that will be easier for investigators to work with.

Materials and Methods

Quantum Dot Synthesis. Commercially available CdSe/ZnS core/shell QDs capped with octadecylamine (ODA) (NN-Labs, 5.8 nm core diameter and 620 nm emission wavelength) were purchased. Previously described⁴⁶ ligand exchange methods were used to prepare water-soluble GSH-QDs. Briefly, ODA-QDs (300 μ L) were precipitated by addition of methanol:acetone (1:1) and separated by centrifugation at 14,000 rpm for 5 min. The ODA-QDs were resuspended in 300 μ L tetrahydrofuran (THF). 30 mg GSH (Cat. number 3541, Calbiochem) was added to 1 mL methanol and adjusted to pH 11.0 with tetramethylammonium hydroxide pentahydrate powder. The ODA-QD THF solution was slowly added to the GSH-methanol solution while stirring, at room temperature in a 4 mL glass vial (VWR) immersed in a mineral oil bath (light white oil, Sigma-Aldrich Inc.) and the mixture was stirred at 60 °C for 2 h on a hotplate/stirrer (VWR). The GSH-QDs were then precipitated with the addition of excess ether (1-2 mL) and centrifuged at 14,000 rpm for 5 min. The supernatant was discarded and GSH-QDs were resuspended in 300

μL 0.01 N NaOH and dialysed using a 5 kD molecular weight cutoff DispoDialyzer filter (Harvard Apparatus Inc.) against excess water (50 mL water, changed once) for 48 h.

scFv Preparation: Preparation of the scFv protein from positive binders and negative controls was performed by removing the M13 gene III fragment of the display vector by digestion of the plasmid with Sall and XhoI, followed by re-ligation of the compatible ends. This manipulation also appends a hexa-histidine tag to the carboxy terminus of the scFv to permit affinity purification of the protein on an immobilized Ni^{2+} resin. The scFvs also contain a FLAG epitope (DYKDDDDKLL) at the amino terminus of the light chain domain to enable secondary detection. After removal of gene III fragment, the scFvs were prepared by growth of the cultures in medium with limiting inorganic phosphate to induce expression from the *phoA* promoter. The cell pellets were lysed with BugBuster™ (Novagen) and the His-tagged scFvs were purified on Ni^{2+} magnetic beads using a Thermo KingFisher instrument to automate bead washing. The scFvs were eluted from the washed beads using PBS containing 300 mM imidazole, and stored at 4°C. Prior to using scFvs in experiments, SDS-PAGE gel was used to confirm presence of scFvs in the sample. The gel was stained with Coomassie Blue (Simply Blue, Invitrogen) and photographed. The approximate concentration of the scFv purified was determined by measuring the absorbance at 280 nm and normalizing it with the reading for pure imidazole used during the above-mentioned elution step.

SEM Imaging. TiO_2 detection limit quantification on the Zeiss Supra 40VP Field Emission SEM was done by preparing coverslips with 50 μL each of 1, 0.1 and 0.01 mg/mL TiO_2 in water pipetted onto an area of 1 cm^2 . EDX spectra were obtained for each of the samples were a discernable peak for Ti was observed for 1 (50 $\mu\text{g}/\text{cm}^2$ TiO_2) and 0.1 mg/mL (5 $\mu\text{g}/\text{cm}^2$ TiO_2) samples but not for 0.01 mg/mL (0.5 $\mu\text{g}/\text{cm}^2$ TiO_2) sample.

Image Stream Flow Cytometry. Anti-FLAG antibody coated commercially available beads (Sigma Aldrich Inc.) were used to coat GSH43 and BiP scFvs passively overnight at 4°C. Beads were collected and centrifuged to remove excess scFvs. The beads were blocked in 2% BSA in TBS for 1 h at room temperature. GSH-QDs at a concentration of 50 nM were added to samples containing scFv-coated beads and to a sample of uncoated beads. QDs were not added to the ‘beads only’ control. QDs were allowed to incubate with the beads for 2 h at room temperature with gentle agitation, after which the beads were washed in TBS with repeated centrifugation and re-suspension. The beads were finally re-suspended in 60 μ L TBS and analyzed using Image Stream under brightfield and fluorescence using appropriate lasers for QDs. Images were analyzed using IDEAS Application software (version 6.0).

Human Skin Processing and NP application. Fresh viable human skin from adult donors was obtained following a mammoplasty or abdominoplasty within hours of surgery. Skin samples were approved for usage by the University of Rochester Research Subjects Review Board (RSRB). The skin was washed thrice with 1X phosphate-buffered saline (PBS) and treated with fungizone (Invitrogen) to remove any microbial contamination. Skin was then processed to remove fat and thin the dermis for easy handling. The samples were placed on gauze in a sterile petri-dish filled with media (5-8 mL) to keep the skin viable. GSH-QDs and TiO₂ NPs were applied on to skin in quantities lesser (0.01 mg/cm^2) than those routinely used for cosmetic testing (0.05 mg/cm^2) by pipetting and spreading them evenly on the epidermal side of the skin. Skin samples were tape stripped (Scotch 3M 3750 clear packing tape, USA) ten times prior to application of GSH-QDs. Each piece of fresh tape was pressed firmly onto the epidermal surface of the skin and removed. GSH-QDs were also injected (50 μ L in 100 μ L deionized water) using

an insulin needle (skin rested with stratum corneum facing upwards) from epidermis to dermis as a positive control sample. Skin samples were placed in the sterile hood for 24 h, after which excess NPs will be wiped off the skin surface using 1X PBS. All the samples were stored at -80 °C until processing for histology.

IHC. Frozen skin was mounted using TEK OCT compound, after which they were sliced (5 µm thickness) on to microscope slides using a cryostat (Thermo Scientific). The epidermis and the dermis were sectioned simultaneously to prevent accidental transfer of NPs to the blade. The slides were fixed in methanol (-20 °C, 10 min) prior to the experiment and dipped in water (Ultrapure™ water, Invitrogen) to remove excess OCT. The slides were washed twice with 1X TBS to wash off excess methanol and a hydrophobic pen was used to create a water-repellent barrier to keep reagents localized on the tissue specimen. The slides were blocked with normal mouse serum for 30 min at room temperature, after which GSH43-scFvs were added to the slides diluted in BSA (10 µg/mL) and allowed to incubate overnight at 4 °C in a humidified chamber. The slides were washed thrice with 1X TBST and incubated with anti-FLAG antibody conjugated to alkaline phosphatase (AP) (Sigma-Aldrich Inc.) for 1 h at room temperature. After washing away excess antibodies, the slides were incubated with BCIP/NBT (KPL) substrate for AP containing 5 mM levamisole (Vector laboratories Inc., CA) for 30 min at room temperature. Levamisole is an endogenous AP inhibitor that enables visualization of AP staining due to the binding of scFv-anti-FLAG AP-tagged antibody alone. Excess substrate solution was washed away with DI water and mowiol (Fluka, #81381, Sigma Aldrich Inc., synthesized in-house) was used as a mounting medium for imaging. The samples were analyzed under a fluorescent microscope (Nikon Eclipse E800 with a Spot RTS Camera) at 40x magnification. Images were captured using brightfield and appropriate fluorescence filters, and analyzed using ImageJ (NIH).

Acknowledgements

The authors thank Michael Tiberio (URMC) for help with protein purification. The authors acknowledge Paivi Jordan (Confocal Microscopy Core, URMC) for her help with the confocal microscope. The authors thank Bob Gelein (URMC) for his help with AAS. The authors acknowledge funding from The Centers for Disease Control and Prevention (1R21OH009970).

References

1. <http://www.bccresearch.com/market-research/biotechnology/nanoparticles-biotechnology-drug-development-delivery-bio113a.html>).
2. M. A. Maurer-Jones, K. C. Bantz, S. A. Love, B. J. Marquis and C. L. Haynes, *Nanomedicine*, 2009, **4**, 219-241.
3. C. O. Robichaud, A. E. Uyar, M. R. Darby, L. G. Zucker and M. R. Wiesner, *Environmental science & technology*, 2009, **43**, 4227-4233.
4. M. Endo, T. Hayashi, Y. A. Kim, M. Terrones and M. S. Dresselhaus, *Philosophical transactions. Series A, Mathematical, physical, and engineering sciences*, 2004, **362**, 2223-2238.
5. Woodrow Wilson Intl. Center for Scholars. . News release: nanotech-enabled consumer products top the 1,000 mark [Internet]. August 25, 2009. Available from: Available at: (<http://www.nanotechproject.org>).
6. S. K. Misra, D. Mohn, T. J. Brunner, W. J. Stark, S. E. Philip, I. Roy, V. Salih, J. C. Knowles and A. R. Boccaccini, *Biomaterials*, 2008, **29**, 1750-1761.
7. A. Elder, S. Vidyasagar and L. DeLouise, *Wiley Interdiscip Rev Nanomed Nanobiotechnol*, 2009, **1**, 434-450.
8. P. V. AshaRani, G. Low Kah Mun, M. P. Hande and S. Valiyaveetil, *ACS nano*, 2009, **3**, 279-290.
9. C. Y. Jin, B. S. Zhu, X. F. Wang and Q. H. Lu, *Chemical research in toxicology*, 2008, **21**, 1871-1877.
10. T. Faunce, K. Murray, H. Nasu and D. Bowman, *NanoEthics*, 2008, **2**, 231-240.

11. F. A. Esteve-Turrillas and A. Abad-Fuentes, *Biosensors & bioelectronics*, 2013, **41**, 12-29.
12. Y. Zhang, Q. Zeng, Y. Sun, X. Liu, L. Tu, X. Kong, W. J. Buma and H. Zhang, *Biosensors & bioelectronics*, 2010, **26**, 149-154.
13. P. V. Kamat, *The Journal of Physical Chemistry Letters*, 2013, **4**, 908-918.
14. Wellesley, *Quantum Dots: Global Market Growth and Future Commercial Prospects*, Report NAN027D, April 2014.
15. N. V. Gopee, D. W. Roberts, P. Webb, C. R. Cozart, P. H. Siitonen, J. R. Latendresse, A. R. Warbitton, W. W. Yu, V. L. Colvin, N. J. Walker and P. C. Howard, *Toxicol Sci*, 2009, **111**, 37-48.
16. N. A. Monteiro-Riviere, K. Wiench, R. Landsiedel, S. Schulte, A. O. Inman and J. E. Riviere, *Toxicol Sci*, 2011, **123**, 264-280.
17. J. P. Ryman-Rasmussen, J. E. Riviere and N. A. Monteiro-Riviere, *Toxicol Sci*, 2006, **91**, 159-165.
18. N. A. Monteiro-Riviere, Zhang, L. W., in *Nanomaterials: Risks and Benefits*, 2009.
19. S. Ravichandran, L. J. Mortensen and L. A. DeLouise, *Nanotoxicology*, 2011, **5**, 675-686.
20. L. J. Mortensen, G. Oberdorster, A. P. Pentland and L. A. DeLouise, *Nano Lett*, 2008, **8**, 2779-2787.
21. R. Alvarez-Román, A. Naik, Y. N. Kalia, R. H. Guy and H. Fessi, *J Control Release*, 2004, **99**, 53-62.
22. L. J. Mortensen, S. Ravichandran, H. Zheng and L. A. DeLouise, *J Biomed Nanotechnol*, 2010, **6**, 596-604.
23. J. G. Rouse, J. Yang, J. P. Ryman-Rasmussen, A. R. Barron and N. A. Monteiro-Riviere, *Nano Lett*, 2007, **7**, 155-160.
24. L. J. Mortensen, S. Jatana, R. Gelein, A. De Benedetto, K. L. De Mesy Bentley, L. A. Beck, A. Elder and L. A. Delouise, *Nanotoxicology*, 2013, **7**, 1386-1398.
25. F. F. Larese, F. D'Agostin, M. Crosera, G. Adami, N. Renzi, M. Bovenzi and G. Maina, *Toxicology*, 2009, **255**, 33-37.

26. F. L. Filon, M. Crosera, G. Adami, M. Bovenzi, F. Rossi and G. Maina, *Nanotoxicology*, 2011, **5**, 493-501.
27. L. Y. Chou, H. C. Fischer, S. D. Perrault and W. C. Chan, *Analytical chemistry*, 2009, **81**, 4560-4565.
28. L. A. DeLouise, *The Journal of investigative dermatology*, 2012, **132**, 964-975.
29. B. Gulson, M. McCall, M. Korsch, L. Gomez, P. Casey, Y. Oytam, A. Taylor, M. McCulloch, J. Trotter, L. Kinsley and G. Greenoak, *Toxicol Sci*, 2010, **118**, 140-149.
30. H. F. Krug, *Angewandte Chemie*, 2014, **53**, 12304-12319.
31. C. Szakal, S. M. Roberts, P. Westerhoff, A. Bartholomaeus, N. Buck, I. Illuminato, R. Canady and M. Rogers, *ACS nano*, 2014, **8**, 3128-3135.
32. W. G. Willats, *Plant molecular biology*, 2002, **50**, 837-854.
33. R. R. Naik, S. J. Stringer, G. Agarwal, S. E. Jones and M. O. Stone, *Nature materials*, 2002, **1**, 169-172.
34. S. R. Whaley, D. S. English, E. L. Hu, P. F. Barbara and A. M. Belcher, *Nature*, 2000, **405**, 665-668.
35. H. Watanabe, T. Nakanishi, M. Umetsu and I. Kumagai, *The Journal of biological chemistry*, 2008, **283**, 36031-36038.
36. T. Hattori, M. Umetsu, T. Nakanishi, S. Sawai, S. Kikuchi, R. Asano and I. Kumagai, *Bioconjugate chemistry*, 2012, **23**, 1934-1944.
37. P. Golec, J. Karczewska-Golec, M. Los and G. Wegrzyn, *Journal of nanoparticle research : an interdisciplinary forum for nanoscale science and technology*, 2012, **14**, 1218.
38. D. Rothenstein, B. Claasen, B. Omiecienski, P. Lammel and J. Bill, *Journal of the American Chemical Society*, 2012, **134**, 12547-12556.
39. T. Hattori, M. Umetsu, T. Nakanishi, T. Togashi, N. Yokoo, H. Abe, S. Ohara, T. Adschiri and I. Kumagai, *The Journal of biological chemistry*, 2010, **285**, 7784-7793.
40. A. Artzy Schnirman, E. Zahavi, H. Yeger, R. Rosenfeld, I. Benhar, Y. Reiter and U. Sivan, *Nano Lett*, 2006, **6**, 1870-1874.

41. B. X. Chen, S. R. Wilson, M. Das, D. J. Coughlin and B. F. Erlanger, *Proceedings of the National Academy of Sciences of the United States of America*, 1998, **95**, 10809-10813.
42. D. Izhaky and I. Pecht, *Proceedings of the National Academy of Sciences of the United States of America*, 1998, **95**, 11509-11510.
43. P. Denny, F. K. Hagen, M. Hardt, L. Liao, W. Yan, M. Arellanno, S. Bassilian, G. S. Bedi, P. Boonthung, D. Cociorva, C. M. Delahunty, T. Denny, J. Dunsmore, K. F. Faull, J. Gilligan, M. Gonzalez-Begne, F. Halgand, S. C. Hall, X. Han, B. Henson, J. Hewel, S. Hu, S. Jeffrey, J. Jiang, J. A. Loo, R. R. Ogorzalek Loo, D. Malamud, J. E. Melvin, O. Miroshnychenko, M. Navazesh, R. Niles, S. K. Park, A. Prakobphol, P. Ramachandran, M. Richert, S. Robinson, M. Sondej, P. Souda, M. A. Sullivan, J. Takashima, S. Than, J. Wang, J. P. Whitelegge, H. E. Witkowska, L. Wolinsky, Y. Xie, T. Xu, W. Yu, J. Ytterberg, D. T. Wong, J. R. Yates, 3rd and S. J. Fisher, *Journal of proteome research*, 2008, **7**, 1994-2006.
44. C. G. Haidaris, J. Malone, L. A. Sherrill, J. M. Bliss, A. A. Gaspari, R. A. Insel and M. A. Sullivan, *J Immunol Methods*, 2001, **257**, 185-202.
45. H. R. Hoogenboom, A. P. de Bruine, S. E. Hufton, R. M. Hoet, J. W. Arends and R. C. Roovers, *Immunotechnology : an international journal of immunological engineering*, 1998, **4**, 1-20.
46. H. Zheng, L. J. Mortensen and L. A. DeLouise, *J Biomed Nanotechnol*, 2013, **9**, 382-392.
47. A. Weir, P. Westerhoff, L. Fabricius, K. Hristovski and N. von Goetz, *Environmental science & technology*, 2012, **46**, 2242-2250.
48. M. Mejare and L. Bulow, *Trends in biotechnology*, 2001, **19**, 67-73.
49. S. Mardyani and W. C. W. Chan, *Journal of Materials Chemistry*, 2009, **19**, 6321-6323.
50. J. A. Lamboy, J. A. Arter, K. A. Knopp, D. Der, C. M. Overstreet, E. F. Palermo, H. Urakami, T. B. Yu, O. Tezgel, G. N. Tew, Z. Guan, K. Kuroda and G. A. Weiss, *Journal of the American Chemical Society*, 2009, **131**, 16454-16460.
51. A. O. Gamer, E. Leibold and B. van Ravenzwaay, *Toxicology in vitro : an international journal published in association with BIBRA*, 2006, **20**, 301-307.
52. N. Sadrieh, A. M. Wokovich, N. V. Gopee, J. Zheng, D. Haines, D. Parmiter, P. H. Siitonen, C. R. Cozart, A. K. Patri, S. E. McNeil, P. C. Howard, W. H. Doub and L. F. Buhse, *Toxicol Sci*, 2010, **115**, 156-166.

53. S. Bass, R. Greene and J. A. Wells, *Proteins*, 1990, **8**, 309-314.
54. G. P. Smith, *Science*, 1985, **228**, 1315-1317.
55. M. Vodnik, U. Zager, B. Strukelj and M. Lunder, *Molecules*, 2011, **16**, 790-817.

Competing financial interests

The authors declare no competing financial interests.

Supporting Information Available

Electronic Supplementary Information (ESI) available: Supplementary data includes figures and detailed methods of various techniques used.

Figure 1

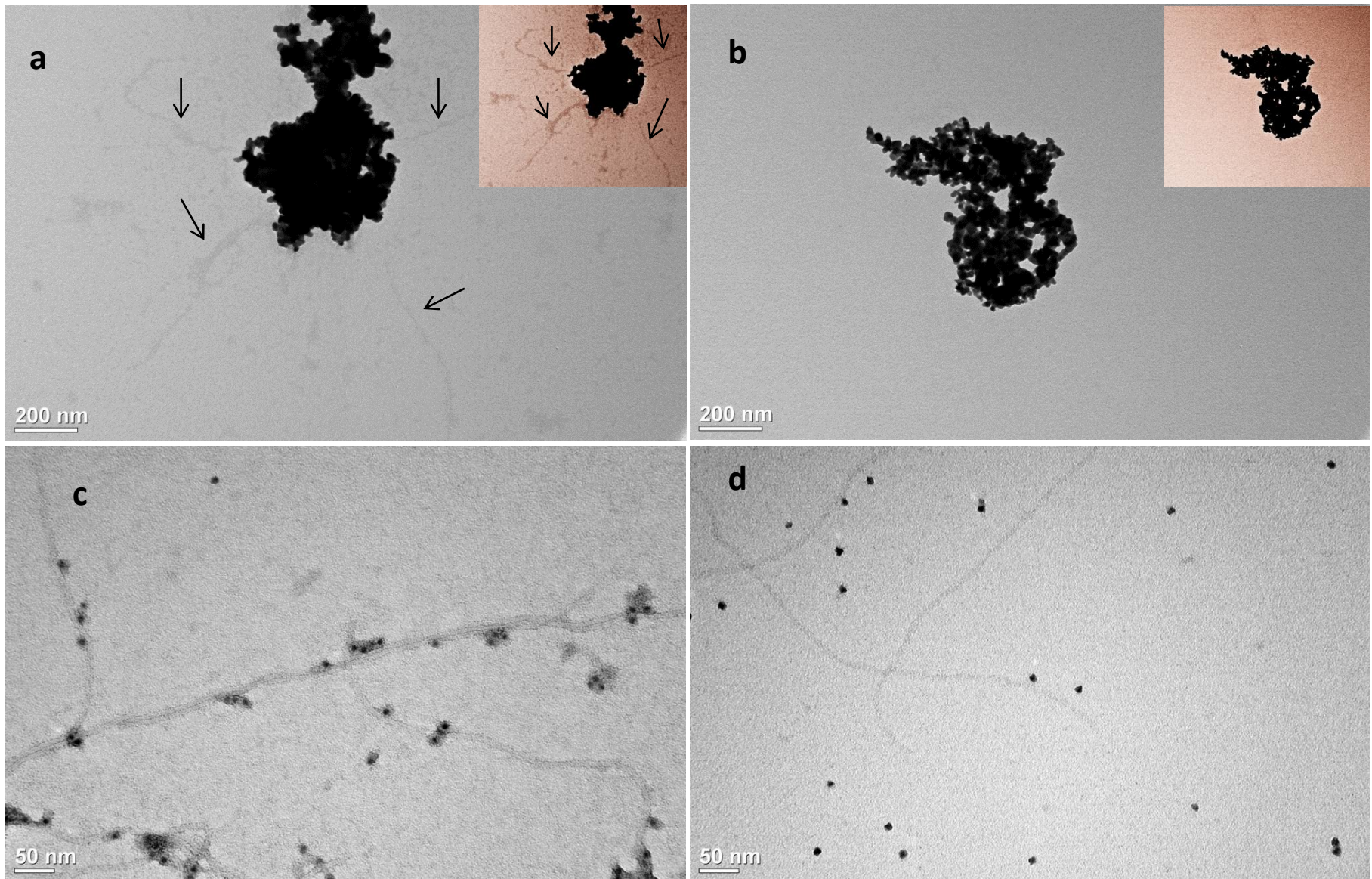


Figure 1: TEM studies of phage binding to respective NP. TEM images showing (a) Ti49 ϕ (black arrows) binding TiO₂ NPs whereas (b) there is no evidence for IL-12 ϕ (negative control) to bind TiO₂ NPs. Scale bar=200 nm. Inset are image enhanced to highlight the phage. (c) GSH43 ϕ exhibit strong association and clustering with GSH-QDs whereas and (d) the negative control IL-12 ϕ show no affinity for the GSH-QD which appear highly dispersed. Scale bar=50 nm.

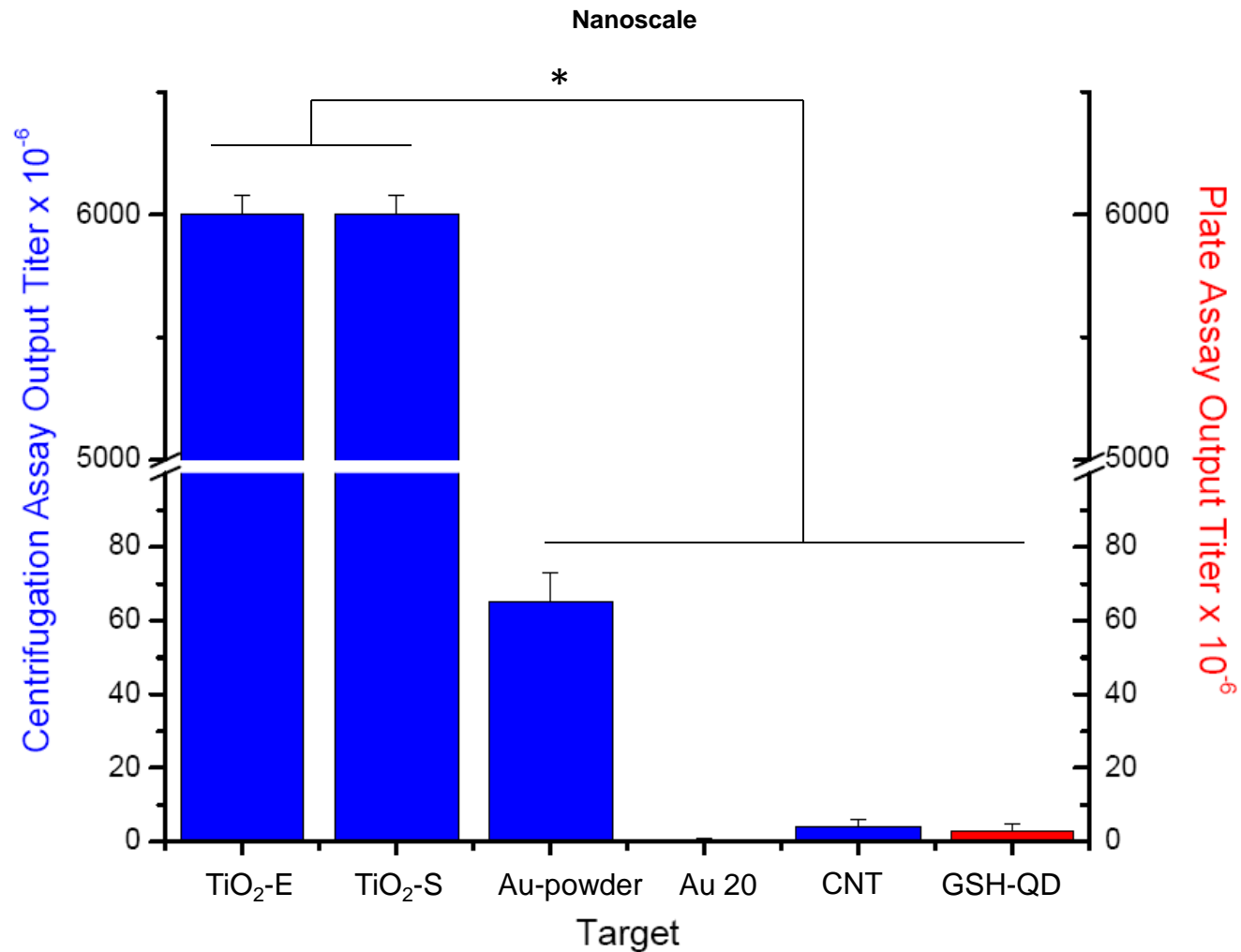


Figure 2a. Results from centrifugation and plate titer assays to examine Ti49 ϕ phage cross reactivity binding to similar and dissimilar materials. Results from the centrifugation titer assay (blue bars) indicates that Ti49 ϕ binds Evonik TiO₂ NPs (TiO₂-E) and TiO₂ NPs from a secondary vendor (Sigma, TiO₂-S) but minimal binding is observed to dissimilar materials including Au-powder particles (Sigma), 20 nm Au (Sigma, Au20), and CNTs (NanoLab, Inc.). Using the plate titer assay the Ti49 ϕ bound the GSH-QDs at background levels. Colonies on the agar plates were counted manually and values plotted on the y-axis. Error bars are the (number of colonies)^{1/2}. Values are statistically significant as observed using a Student's t test ($p < 0.001$).

Nanoscale

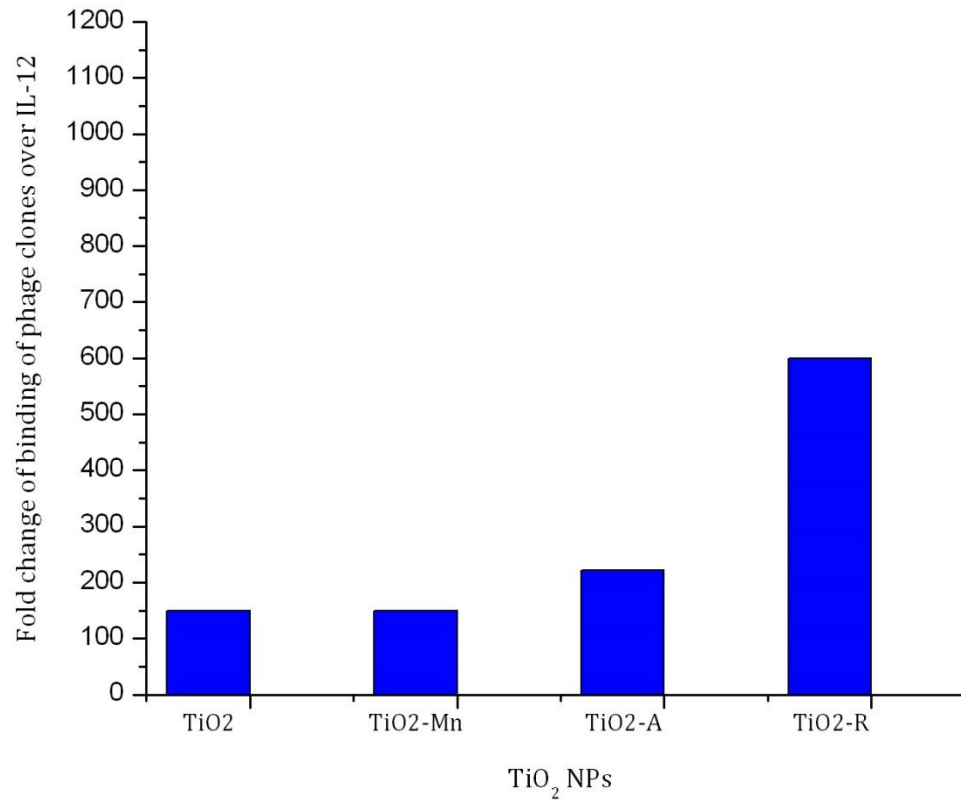


Figure 2b. Binding of Ti49 ϕ to TiO₂ NPs. Binding of Ti49 ϕ to different TiO₂ NPs varying in composition and source. A) Using a centrifugation titer assay, Ti49 ϕ was found to bind TiO₂-Mn (Sigma Aldrich Inc.) similar to TiO₂ NPs (Evonik, P25), bound TiO₂-R higher (by 3-fold), and bound TiO₂-A by ~1.5-fold more than the other TiO₂ NPs.

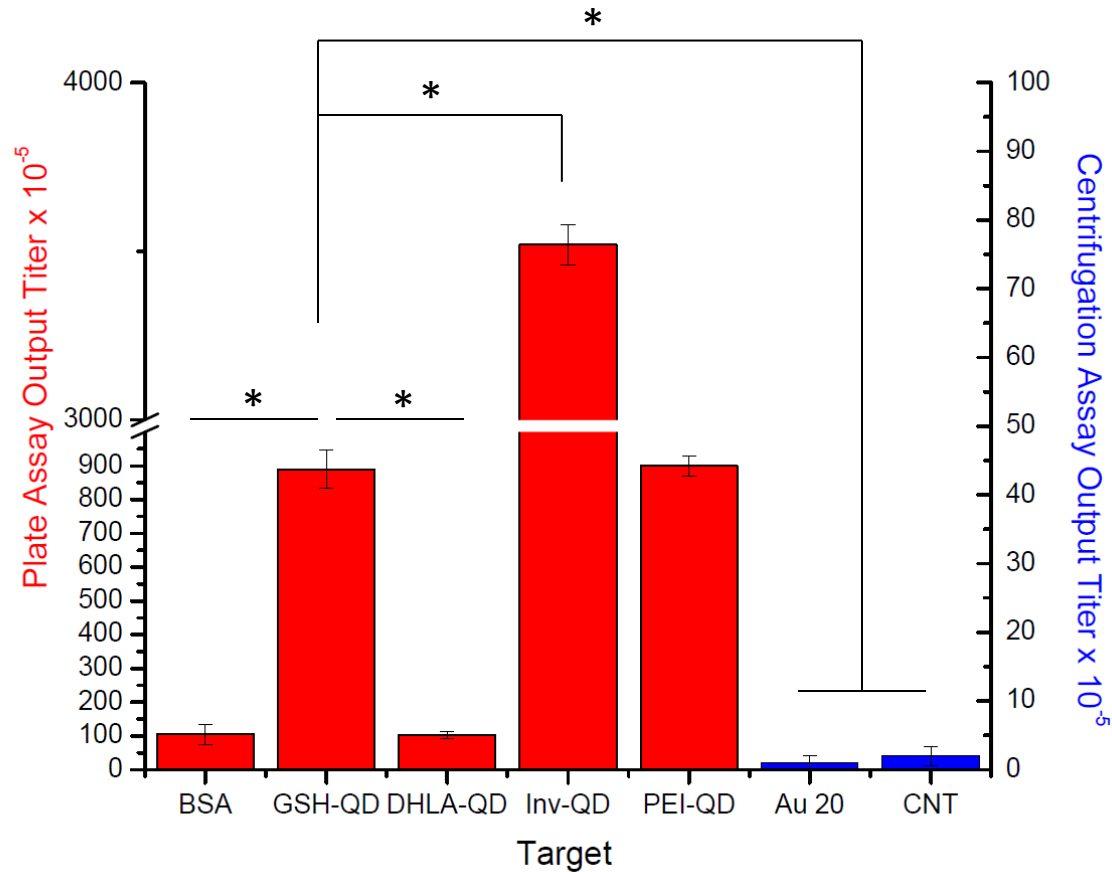


Figure 2c. Results from centrifugation and plate titer assays to examine GSH43 ϕ phage cross reactivity binding to similar and dissimilar materials. Plate titer assay results (red bars) indicate that the GSH43 ϕ clone exhibits strong binding to negative charged GSH-QDs (~9-fold over the BSA-only, $p=0.0035$, no QD control sample), to negative charged Invitrogen ($p=0.0005$) and positive charged PEI-QDs ($p=0.8$, not significant). However, minimal binding is seen to negative charged DHLA-QDs ($p=0.0028$) and also to dissimilar materials including 20 nm Au NPs and CNTs ($p=0.002$) determined by the centrifugation titer assay (blue bars). Colonies on the agar plates were counted manually and values plotted on the y-axis. Error bars are the (number of colonies)^{1/2}. Statistical analysis was done using Student's t-test and values were considered significant if $p<0.05$. All samples were compared to binding of GSH43 ϕ to GSH-QDs to measure significance.

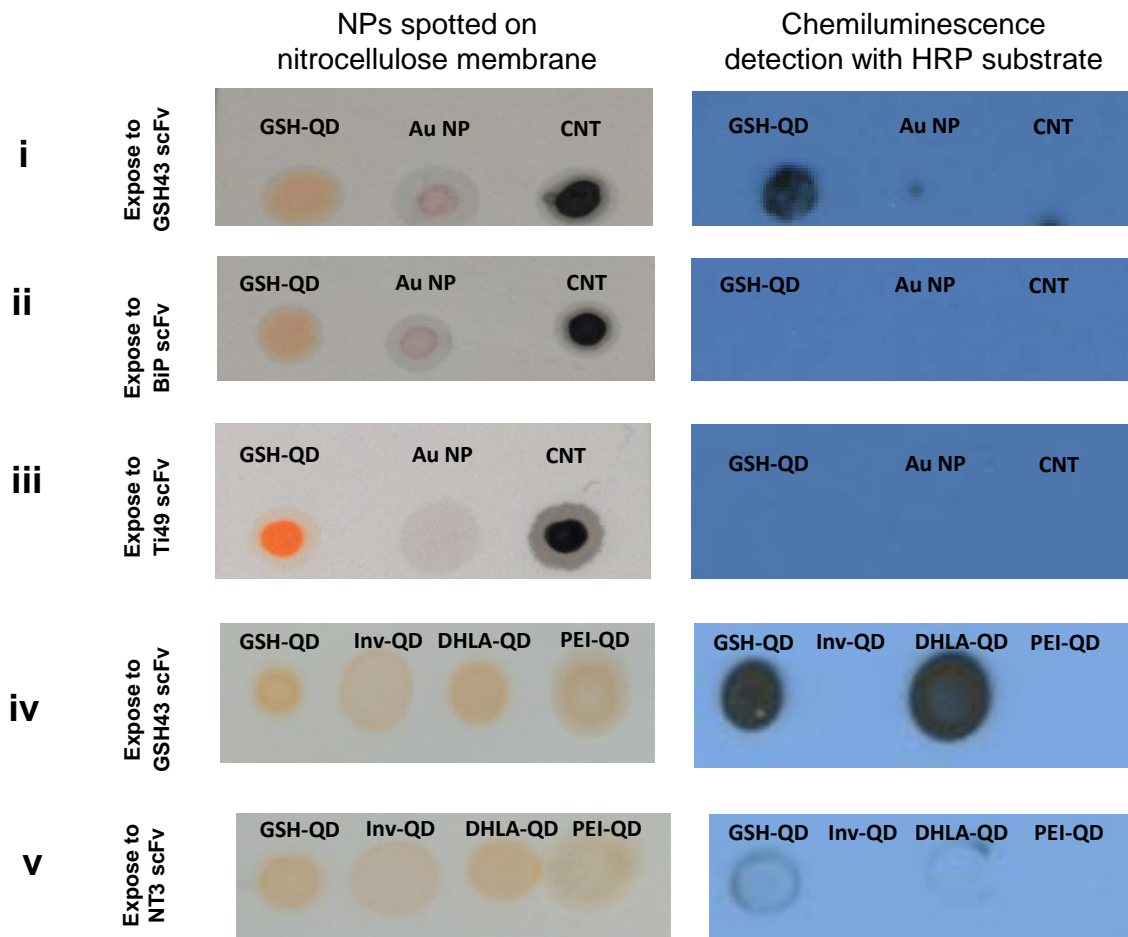
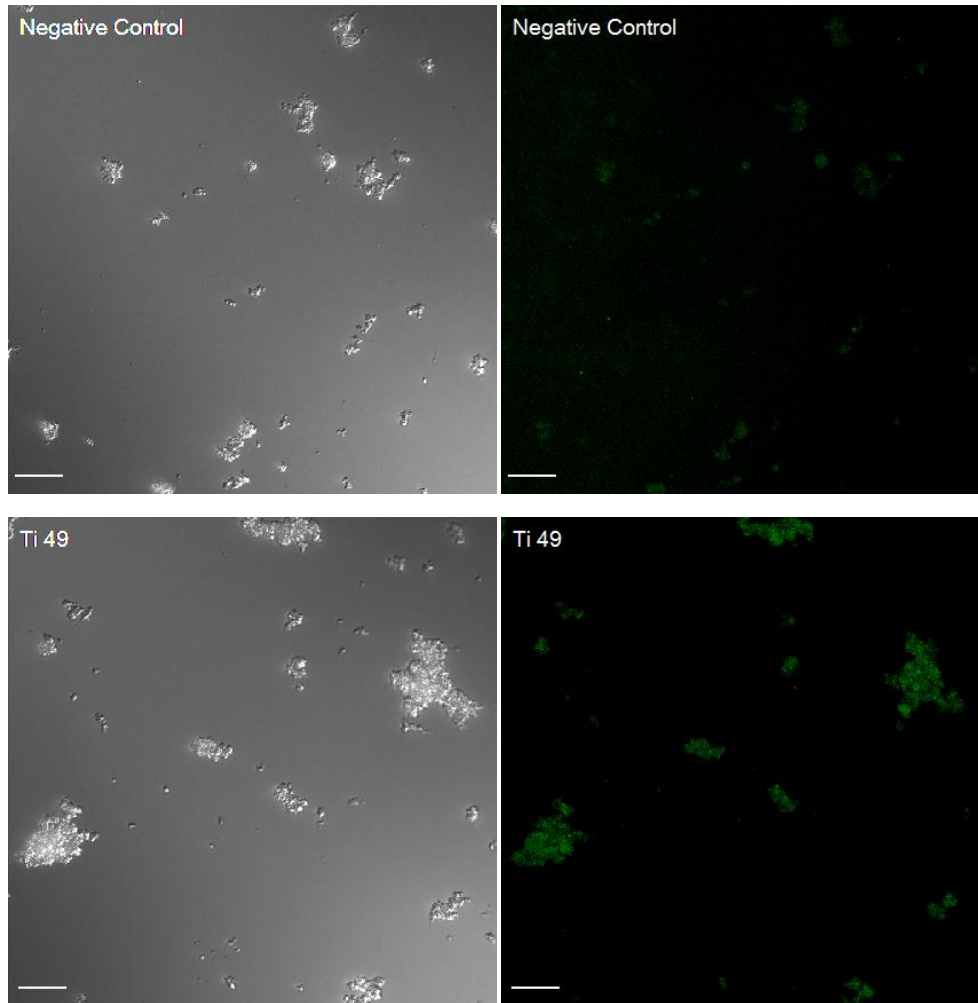


Figure 3a: Dot blots investigating scFv binding to similar and dissimilar materials. For dissimilar materials, spots on a nitrocellulose membrane (left column) showing GSH-QDs (**orange**), Au NPs (**pink**) and CNTs (**black**) spots. Chemiluminescence detection of scFv binding with HRP (right column). Results show that **(i)** GSH43-scFv (5 $\mu\text{g}/\text{mL}$) binds GSH-QDs but not Au NPs and CNTs, **(ii)** negative control BiP-scFv (5 $\mu\text{g}/\text{mL}$) and **(iii)** Ti49-scFv (5 $\mu\text{g}/\text{mL}$) do not bind any of the NPs. For similar materials, GSH-QDs, Invitrogen ITKTM 565-QDs (Inv-QDs), DHLA-QDs, and PEI QDs were spotted on a nitrocellulose membrane (left column). Upon chemiluminescence detection of scFv binding using HRP (right column), results show that **(iv)** GSH43-scFvs bind GSH-QDs and DHLA-QDs at 5 $\mu\text{g}/\text{mL}$, but not Inv-QDs and PEI-QDs whereas **(v)** NT3 negative control scFvs show faint background staining at the same concentration.

i



ii

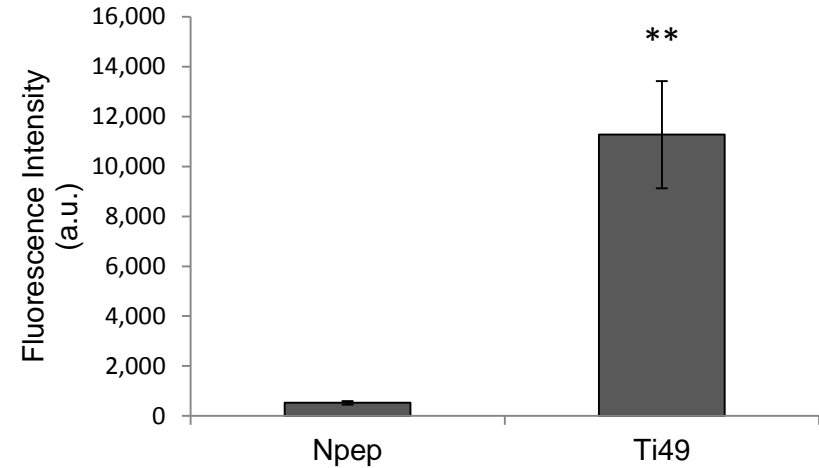


Figure 3b: Brightfield and confocal images investigating the binding of Ti49-scFvs to TiO₂ NPs immobilized on a glass slide using FITC-conjugated anti-FLAG secondary antibody detection. **(i)** Representative images of negative control Npep-scFv showing minimal binding to TiO₂ NPs (**row 1**), whereas Ti49-scFvs shows strong binding to TiO₂ NPs (**row 2**). Scale bar=20 μm. **(ii)** Quantitative analysis of the integrated fluorescence intensity shows significant difference in the Ti49-scFv treated sample compared to negative control Npep-scFv. Data shown is average of three ROIs from the images. Error bars indicate SEM. **p=0.0075 using student's unpaired t-test.

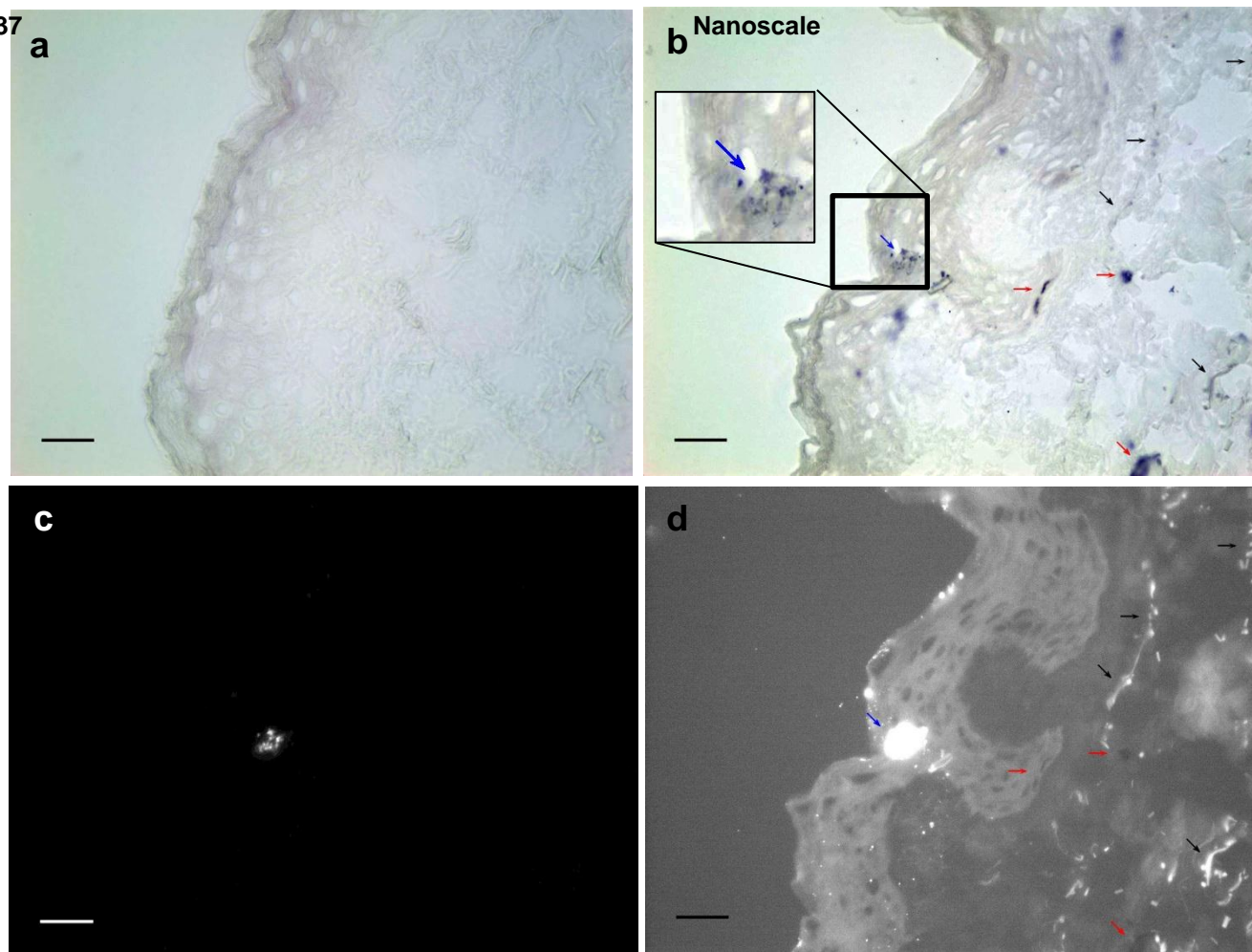


Figure 4

Figure 4: QD detection in *ex vivo* human skin using GSH43-scFv. Skin slices were pretreated with levamisole to reduce endogenous phosphatase activity. **(a)** Control skin sample without GSH-QD exposure showing an absence of AP staining indicating a lack of GSH43-scFv non-specific binding to skin. **(b)** Brightfield image of skin sample exposed to GSH-QDs for 24 h showing numerous areas with strong AP staining (**black, blue, and red arrows**). Inset shows an area of high AP staining (**blue arrow**) in the epidermis that correlates with high QD presence as seen under **(c)** fluorescence imaging, exposure 1.642 s. **(d)** Applying a threshold to enhance the fluorescent signal shows that some of the areas with strong AP staining (**black arrows**) co-localize with QD fluorescence, whereas other areas (**red arrows**) indicate potential presence of QDs that are not visible under the fluorescence exposure conditions used. This suggests the ability of GSH43-scFv to detect the presence of QDs that may otherwise being undetectable in skin. This was confirmed with LCM studies. Scale bar=50 μm .

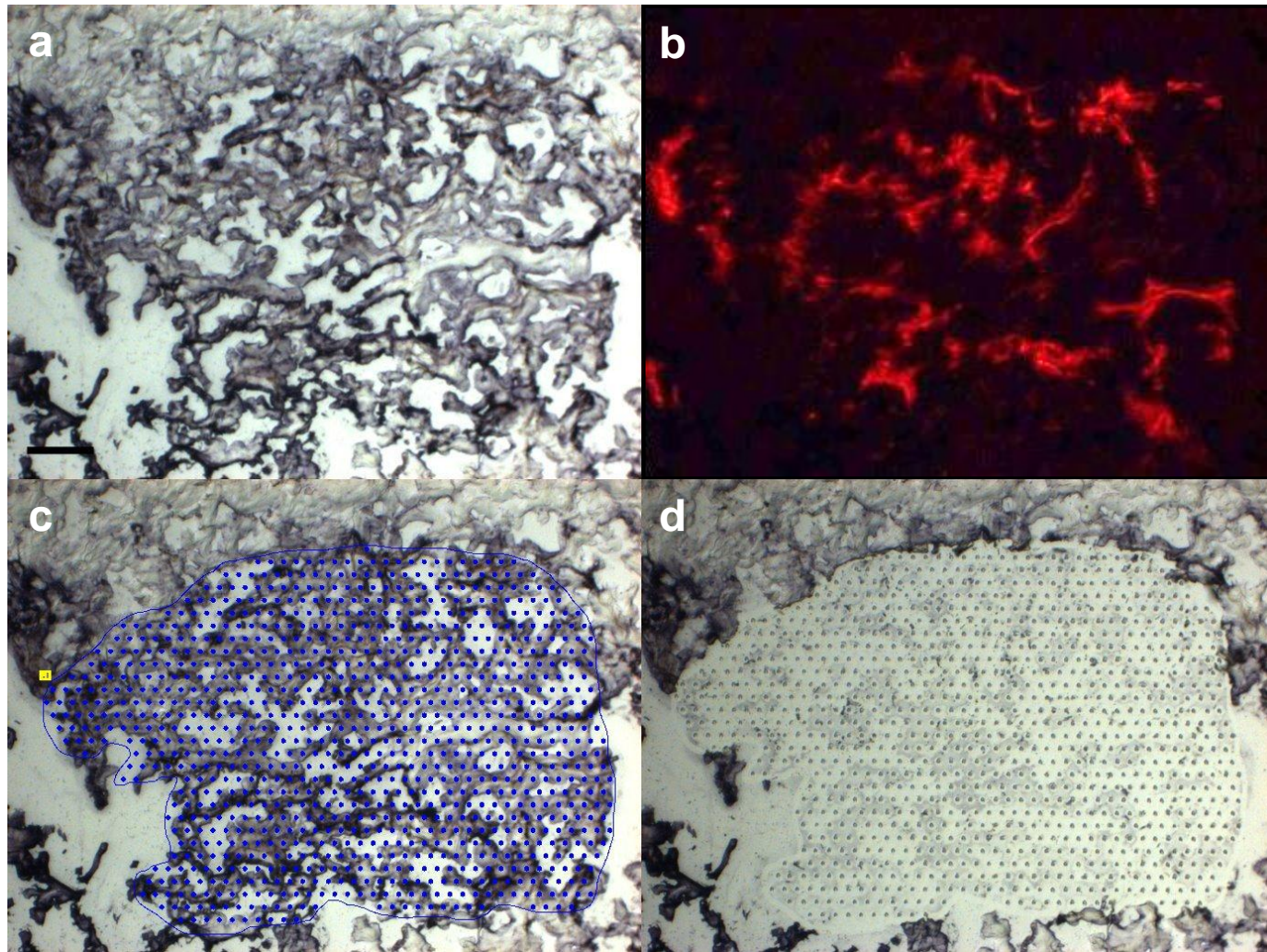


Figure 5: LCM imaging microscopy to confirm presence of GSH-QDs in areas of high AP staining. Representative skin sample containing QDs injected showing (a) dark bluish-purple staining indicating binding of GSH43-scFvs detected by AP. (b) Fluorescence image of skin sample before dissection showing QD presence. (c) Portions of stained areas were marked for cut and captured onto adhesive tube caps using LCM, and processed for AAS. (d) The portion of skin remaining after capture. Scale bar=50 μ m.

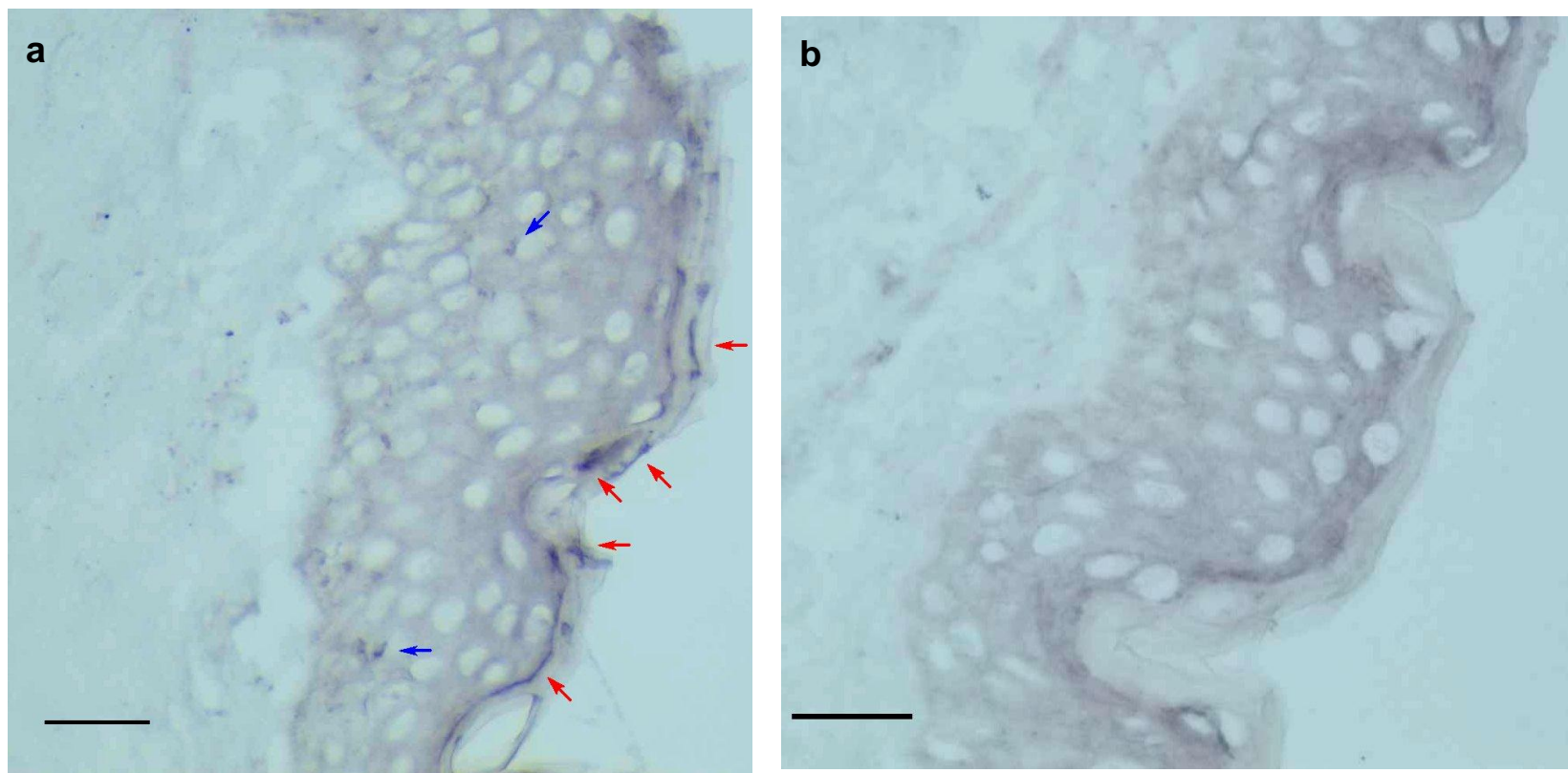
Nanoscale
Figure 6

Figure 6: Detection of TiO₂ using Ti49-scFv in human skin *ex vivo*. Representative images of **(a)** TiO₂ applied on epidermis of intact skin, **red arrows** indicates AP staining due to binding of Ti49-scFv to TiO₂ NPs. **Blue arrows** indicate AP staining, which could potentially be TiO₂ particles penetrated through skin to the dermis. **(b)** Control sample with no TiO₂ applied and upon exposure to Ti49-scFvs, no non-specific binding (no AP staining) was observed. Scale bar=50 μm.